Apparent nitrous acid dissociation across environmentally relevant temperatures in freshwater and seawater

Benedict Borer, Eric Bi, Ryan J. Woosley, Andrew R Babbin*

Department of Earth, Atmospheric and Planetary Sciences, Massachusetts Institute of Technology, Cambridge, MA 02139, USA

*Corresponding author: babbin@mit.edu

Running head: Apparent nitrous acid pK_a in fresh and seawater

Significance statement

Nitrite (NO_2^-) plays a key role in nitrogen biogeochemistry and ecosystem health across aquatic environments, from lakes and rivers to the open ocean to sediments. While biological transformations of nitrite have been studied meticulously, spontaneous abiotic reactions such as the acid-base equilibrium between nitrite and its conjugate nitrous acid (HNO_2) have rarely been evaluated across environmentally relevant conditions. These are critical to assessing nitrogen cycling in all systems. In this manuscript, we report the pK_a of nitrous acid in both freshwater and seawater at temperatures ranging from 5 °C to 35 °C using potentiometry-based titration. Our measured pK_a values fit well within the range of previously reported pK_a values, although notably, past measurements have been mostly restricted to 25 ºC in freshwater. To our knowledge, we provide the first attempt to strategically measure the pK_a of nitrous acid in freshwater across environmentally relevant temperatures, and the very first measurements in seawater at any temperature.

Due to the importance of nitrogen for primary productivity and anoxic nutrient cycling, and the pervasive influence of nitrite on organisms and ecosystem function, our results have broad implications across aquatic systems that are of interest to the L&O community. In addition, similar data that were published in L&O have proven to be consequential for our understanding of aquatic systems such as the dissociation of carbonic acid (Mehrbach et al., 1973, L&O 18, 897-907), phosphoric acid (Kester & Pytkowicx, 1967, L&O 12, 243–252), and hydrogen sulfide (Millero et al., 1988, L&O 33, 269–274), and we would thus be excited to publish our data in L&O.

Author contribution: CRediT

Conceptualization: BB, ARB
Methodology: BB, RJW, ARB
Software: BB
Formal analysis: BB, RJW, ARB
Investigation: BB, EB, ARB
Data Curation: BB, ARB
Writing - Original Draft: BB, EB, RJW, ARB
Writing - Review & Editing: BB, EB, RJW, ARB
Visualization: BB
Funding acquisition: BB, RJW, ARB

Abstract

Nitrite is a ubiquitous compound found across aquatic systems and an intermediate in both the oxidative and reductive metabolisms transforming fixed nitrogen in the environment. Yet, the abiotic cycling of nitrite is often overlooked in favor of biologically mediated reactions. Here we quantify the apparent acid dissociation constant (pK_a) between nitrous acid and nitrite in both freshwater and seawater systems across a range of environmentally-relevant temperatures (5–35 ºC) using potentiometric-based titration. We find substantial effects of both salinity and temperature on the pK_a, with colder and fresher water manifesting higher values and thus a greater proportion of protonated nitrite at any given pH. Because nitrous acid is unstable and decomposes to nitric oxide, a toxic free radical gas but also a potential antioxidant and biological signaling compound, the implications for the nitrous acid pK_a on ecosystem function are broad.

Introduction

Nitrogen biogeochemistry in the natural environment is commonly considered a critical variable controlling ecosystem productivity (Gruber and Galloway, 2008). Nitrite (NO_2^-) is a central compound in this important nitrogen cycle and an intermediate in both the oxidative nitrification and reductive denitrification and dissimilatory reduction to ammonium processes (Babbin et al., 2020, 2021). It further is an intermediate in assimilatory nitrate reduction by phytoplankton and other microbes. Nitrite has been well described across the ocean, accumulating at predictable depth horizons below the euphotic zone (the primary nitrite maximum, PNM) (Lomas and Lipschultz, 2006; Zakem et al., 2018; Ciccarese et al., 2023), at anoxic marine depths in the oxygen deficient zones (the secondary nitrite maximum, SNM) (Ulloa et al., 2012; Babbin et al., 2014, 2017, 2020), and sometimes in marine sediments at the interface between oxic and anoxic layers (Zhao et al., 2023). Furthermore, global lakes ranging from large temperate basins to confined polar meromictic lakes can exhibit nitrite accumulation globally both in the water column and in underlying sediments, often elevated under eutrophic and low oxygen conditions (Vincent et al., 1981; Lee et al., 2004; Powers et al., 2017).

While the biological transformations of nitrite have been measured across many marine and lacustrine systems, the acid-base equilibrium (Eq. 1) between nitrite and its conjugate nitrous acid (HNO_2) has rarely been evaluated. Indeed, as a weak acid, nitrite can exist in both a protonated and de-protonated form dictated by the specific pH of the system. In this capacity, nitrite acts like the weak base ammonia rather than the very strong nitric acid which completely dissociates to nitrate and a proton under all environmentally relevant conditions. Yet, unlike ammonia (Khoo et al., 1977; Clegg and

Whitfield, 1995), the equilibrium constant for nitrite has not been assessed across environmentally relevant temperatures or in seawater. Determining this constant, K_a, or its more common negative-logarithm transform, pK_a, dictates the speciation between nitrous acid and nitrite as a function of pH, where {*i*} indicates the activity of compound *i*, often simplified as a concentration (Eq. 2).

$\mathrm{HNO_2} \overset{K_a}{\leftrightarrow} \mathrm{H^+} + \mathrm{NO_2^-}$	*Eq. 1*
$pK_a = \mathrm{pH} - \log_{10}\left(\frac{\{\mathrm{NO_2^-}\}}{\{\mathrm{HNO_2}\}}\right)$	*Eq. 2*

The speciation of nitrite in particular matters because protonated nitrous acid is unstable and decomposes spontaneously to the free radicals nitric oxide (•NO) and nitrogen dioxide ($•NO_2$) (Eq. 3). Both compounds are NOx gases contributing to the formation of smog and acid rain (Stephens et al., 1956), and the formation and destruction of ozone (Crutzen, 1979). The decomposition of nitrous acid thus produces these compounds, which can be toxic and/or antioxidants and signaling compounds depending on the conditions and organisms considered (Vardi et al., 2006; Wilbert and Newman, 2022; Abada et al., 2023). Regardless of the pathway, the generation of these gases could result in abiotic denitrification and the ultimate loss of nitrite from an aqueous system. Indeed, the pH-dependence of nitrite toxicity for bacterial denitrifiers has been recently shown (Lilja and Johnson, 2016; Borer et al., 2020; Ciccarese et al., 2022). Nitrogen dioxide can further disproportionate back into nitric and nitrous acids, which recovers a proton and lowers the system's pH (Eq. 4). Given the differences in stability of

nitrous acid and nitrite, this speciation is critical in assessing nitrite's role in aquatic systems.

$2HNO_2 \overset{K_1}{\leftrightarrow} NO + NO_2 + H_2O$	*Eq. 3*
$2NO_2 + H_2O \overset{K_2}{\leftrightarrow} H^+ + NO_3^- + HNO_2$	*Eq. 4*

Previous measurements of nitrous acid's pK_a have predominantly been reported for freshwater at 25 ºC, which comprises a small fraction of all natural waters. The previously determined values typically range between 2.8 and 3.4, with differences dictated primarily by the accuracy and precision of the utilized systems. Furthermore, the reaction kinetics of nitrous acid decomposition (K_1) and nitrogen dioxide disproportionation (K_2) have been determined as second-order with respect to the reactants. The kinetic constants of these two reactions have been described at several temperatures in freshwater, permitting extrapolation to other temperatures via the Arrhenius equation. Here we set out to determine the pK_a of nitrous acid through a series of titrations across temperatures between 5 and 35 ºC at both freshwater and seawater salinities to generate the essential data for fully assessing nitrite's transformations in most aquatic environments and developing the mechanisms underlying its toxic role.

Methods

Preparation of stock solutions

All glassware was washed three times with ultra-pure reverse osmosis water (milliQ) and dried overnight at 70 °C in a convection oven before use. Hydrochloric acid

at a concentration of 1 M (molar, mol L^{-1}) was used as the titrant. The titrant was prepared by dilution of 37% concentrated HCl (ACS Grade, VWR Chemicals BDH). Nitrite stock solutions in pure water (0.1 M, 1000 mL) were made using sodium nitrite (Sigma-Aldrich, CAS# 7632-00-0). For the seawater titrations, synthetic seawater devoid of carbonate and boric acid was used to restrict any interference of the natural seawater buffering capacity. The composition of the synthetic seawater (Millero, 2013) is shown in Table 1. The sodium chloride was adjusted to account for the sodium added from the $NaNO_2$ to maintain the same ionic strength as natural seawater. The synthetic seawater was mixed at least 48 hours prior to the first titration. Finally, 6.900 g of sodium nitrite was added to a 1 L volumetric cylinder and filled with synthetic seawater.

Titration method

Titrations were performed in a 250 mL jacketed reaction beaker (Ace Glass Incorporated, Vineland, NJ). The beaker was connected to a thermostatic water bath (AD 7LL R-20 Refrigerated Circulating Bath, VWR) to control the temperature during the titration to within ±0.07 °C. The temperature was monitored and recorded during the titration using a RTD PT100 thermometer calibrated to ±0.01 °C (Omega Engineering PR-11-2-100-1) inserted into the titrate. The titrate was continuously stirred using a magnetic stir bar at 300 rpm on a magnetic stir plate (PC-410D, Corning). A Metrohm Electrode Plus (6.0262.100, Metrohm) was used to measure the resulting electromotive force (EMF) during the titration. The electrode was connected to a custom high-impedance voltage-follower amplifier to buffer the EMF of the glass electrode assembly such that it can be read accurately using a digital voltmeter (custom-built by Andrew Dickson, UCSD). We recorded the EMF measured by the electrode-amplifier system and the temperature in

142 the titrate using a digital voltmeter readable to 0.01 mV (34970A Data Acquisition/Data
143 Logger Switch Unit, Keysight Technologies). The electrode, temperature sensor, and
144 injection needle were inserted into the titrate through a custom, 3D-printed lid to restrict
145 evaporation and thermal exchange during the titration. Both the EMF and temperature
146 within the titrate were recorded at 4-second intervals. For each titration, the nitrite stock
147 solution (the titrate) was prewarmed to the desired temperature in the volumetric flask.
148 Approximately 100 g of the nitrite titrate solution was transferred to a glass beaker,
149 the exact amount determined by weight. After the titrate reached a stable temperature (as
150 monitored by the temperature sensor) the titrant (1 M HCl solution) was injected into the
151 reaction vessel using a programmable syringe pump (PHD 22/2000 Advance Syringe
152 Pump, Harvard Apparatus). The syringe pump injected 100 µL of titrant into the reaction
153 vessel every 28 s, allowing for equilibration and a total of 7 measurements in between
154 injections. The injection interval was chosen as a multiple of the recording interval and
155 based on preliminary experimental results that verified a stable EMF within that time
156 frame. A total of 15.1 mL of titrant was injected into the reaction vessel over 70 minutes
157 during which both the EMF and temperature were recorded (Fig. 1a provides a
158 representative EMF curve measured during the titration). Experiments were conducted at
159 target temperatures of 5–35 °C in 5 °C intervals (a total of 7 temperatures) with four
160 replicates at each temperature. Experiments were performed for both freshwater (no salt
161 beyond 0.1 M $NaNO_2$) and seawater.

162 *Electrode calibration*

163 The EMF of reference materials was measured for each temperature and salinity
164 before the first replicate and after the last replicate to account for any electrode drift (none

existed). For freshwater titrations, the EMF of certified reference buffers at pH 2, 4, 7, and 10 (BDH5010, BDH5018, BDH5046, and BDH5072, respectively, VWR Chemicals BDH) were measured at the specific temperature used for the titration. The measured EMF is then related to the pH_{NBS} certified by the manufacturer at the respective temperature using a linear regression. However, due to unreliable EMF measurements for the 10 °C calibration and unavailable certified pH_{NBS} values at 5 °C for the pH 2 buffer, regressions for the calibration intercept (Fig. 2a) and slope (Fig. 2b) as functions of temperature were performed. The resulting linear regressions are shown in Eq. 5 to Eq. 7, with temperature *t* in ºC.

$\mathrm{EMF}_{Measured,t} = q_{(t)} + m_{(t)} \times \mathrm{pH}_{NBS,certified,t}$	*Eq. 5*
$q_{(t)} = 371.08 + 1.57 \times t_{(°C)}\ ;\ R^2 = 0.997$	*Eq. 6*
$m_{(t)} = -52.41 - 0.24 \times t_{(°C)}\ ;\ R^2 = 0.998$	*Eq. 7*

For seawater titrations, Tris Buffer Solution in Synthetic Seawater (TRIS) (DelValls and Dickson, 1998; Paulsen and Dickson, 2020) obtained from Andrew Dickson (UCSD; Batch T42-0035) pre-equilibrated to the titration temperature were used for a one-point calibration (the measured EMF corrected to pH 0 as a function of temperature is shown in Fig. 2a). The electrode exhibited Nernstian behavior within accepted uncertainty (Fig. 2b). For all freshwater titrations, intercepts and slopes from the regression (Eq. 5) were used whereas only the slope of the regression was used for the seawater titrations in combination with the measured intercept EMF. All calibration data for the different experimental conditions are shown in Table 2.

It is important to note that the electrode is calibrated to different pH scales for the freshwater and seawater experiments. For freshwater, the electrode is calibrated on the National Bureau of Standards (NBS) activity scale ($pH_{NBS} = -\log_{10}\{H^+\}$). This scale is only defined for dilute solutions and is not applicable in high ionic strength media such as seawater. For reasons explained in great detail elsewhere (Dickson et al., 2015), seawater measurements are calibrated on the total scale ($pH_T = [H^+]_{free} + [HSO_4^-]$). The conversion between the scales is ill-defined and because freshwater and seawater communities tend to use their respective scales, and thus we report the pK_a determined here on their respective scales.

Determination of the pK_a

For each titration, the recorded data point prior to the first injection of the titrant was identified manually. Subsequently, the measurement prior to the next injection was extracted as every 7th data point (Fig. 1b) and used for downstream analysis. The difference in EMF between subsequent injections was used as a numerical derivative to find a first approximation of the inflection points to identify the endpoint (where the amount of titrant added exactly neutralizes the titrate) and location of the half equivalence point (where exactly half of the nitrite is converted to nitrous acid and thus the pK_a equals the measured pH, see Fig. 1a). We subsequently used 10 to 30 data points around the numerically identified half equivalence point to fit a quadratic curve and find the exact half equivalence point via the derivative. Replicates that showed an unstable EMF profile during any part of the titration, indicative of ambient electrostatic interference, were discarded from the analysis. The final number of replicates used in both the freshwater and seawater analysis is shown in Table 3.

Results and discussion

Extracted EMF at the titration half equivalence point

For each titration condition (temperatures ranging from 5 °C to 35 °C in both freshwater and seawater) we extracted the measured EMF at the half equivalence point of the titration (where the pH equals the pK_a of nitrous acid) as described in the Methods section. The resulting EMF as a function of temperature is shown in Fig. 3a and the underlying data including the number of replicates are presented in Table 3. The measured temperature in the titrate is very close to the desired value (Fig. 4), with a slight elevation at 5 °C for both the freshwater and seawater conditions. This is because the injected titrant is at room temperature (~20 °C) and injection further increases the temperature of the titrate due to exothermic dilution (Table 3, Fig. 4a). At 20 °C, exothermic dilution elevates the temperature slightly (Fig. 4b), whereas the exothermic dilution effect counteracts the potential cooling of the room-temperature titrant at 35 °C (Fig. 4c). The extracted EMF values at the half equivalence points show excellent reproducibility across the individual replicates for both the freshwater and seawater experiments. When comparing freshwater and seawater EMF, there is a comparable trend as a function of temperature, offset by 13.23 ± 0.5 mV (mean ± std). There is no apparent pattern in the standard deviation between the extracted EMF at the half equivalence point, and this variation is within one order of magnitude of the reported accuracy of the electrode for many conditions (±0.01 mV).

Nitrous acid dissociation constants

We convert the EMF at the half equivalence point for each experimental condition to the pK_a using the calibration procedure outlined in the Methods. The resulting pK_a for both the freshwater and seawater experiments are shown in Fig. 3b, with the change between pK_a at 5 ºC and 35 ºC being 0.1 and 0.5 pH units lower for freshwater and seawater, respectively. Due to the calibration procedures, the pK_a of the freshwater experiments is on the NBS scale whereas the pK_a of the seawater experiments is on the total scale. Our experimental results fall within the range of the previously determined pK_a of nitrous acid reported in the literature as shown in Fig. 3. The dissociation constants of nitrous acid from the literature are presented in Table 4, which are all determined for low ionic strength solutions and thus only comparable to our freshwater conditions. With few exceptions, dissociation constants for nitrous acid were uniquely determined at 25 °C. Overall, our results align with previously determined values (Table 4) but show a slightly lower pK_a when compared to the previously determined values at 25 °C ($pK_{a,Avg}$ of 3.28 ± 0.64 compared to a $pK_{a,NBS}$ of 3.14 ± 0.001 in our measurements). Since previously measured pK_a values are predominantly determined at 25 °C, we cannot compare our established relationship between the pK_a and temperature with the literature.

Calculation of thermodynamic parameters of ionization

We further calculate thermodynamic parameters of ionization (the change in enthalpy, heat capacity, and entropy) from the relationship between the measured pK_a and temperature (Bates and Calais, 1981; Millero et al., 1988). By combining the equations for the Gibbs free energy at equilibrium (Eq. 8) and the calculation of the same Gibbs energy of ionization from the enthalpy and entropy of ionization (Eq. 9) (Ives and

Moseley, 1976), we obtain an expression for the pK_a as a function of temperature (Eq. 10). By fitting this equation to our data, we can extract thermodynamic parameters from each of the fitted parameters (Eq. 11). In all these equations, the temperature T is in Kelvin.

$\Delta G^o = \ln(10)\, R\, T \times pK_a$	*Eq. 8*
$\Delta G^o = \Delta H_0^o + \Delta C_P T - T\Delta S_0^o - \Delta C_P T \ln(T)$	*Eq. 9*
$pK_a = \frac{1}{\ln(10)\, R}\left(\frac{\Delta H_0^o}{T} - \Delta C_P \ln(T) + (\Delta C_P - \Delta S_0^o)\right)$	*Eq. 10*
$pK_a = \frac{A}{T} + B \ln(T) + C$	*Eq. 11*

We use two different methods to fit Eq. 11 to our data: a least-squares approach using the Matlab built-in 'trust-region-reflective' algorithm and the Sigma plot method (Ives and Moseley, 1976). Our data show a good fit to the equation for the freshwater and seawater pK_a both when using the least squares approach (R^2 of 0.985 and 0.986, respectively) and the Sigma plot method (R^2 of 0.945 and 0.971, respectively). The curves fitted to the freshwater and seawater pK_a have different coefficients A, B, and C as expected since the thermodynamic parameters are functions of the salinity (Millero, 1995). The fitted coefficients and derived thermodynamic parameters concerning the change of enthalpy, heat capacity, and entropy from ionization are shown in Table 5. There are only slight differences between the extracted parameters when comparing the least-squares approach with the Sigma plot method. Since the least-squares approach shows a slightly better fit for both the freshwater and seawater conditions, we propose the following

equations to calculate the pK_a for nitrous acid in freshwater (Eq. 12) and seawater (Eq. 13) as a function of the temperature in K:

$$pK_{a,NBS} = \frac{11328}{T} + 37.613 \ln(T) - 249.16$$	*Eq. 12*
$$pK_{a,T} = \frac{15168}{T} + 48.245 \ln(T) - 322.94$$	*Eq. 13*

Relevance for biological systems

The pK_a we determine for nitrous acid is, as expected, much lower than the pH of most aquatic systems. Yet, two factors still demand quantifying the pK_a across environmental conditions: (1) regardless of the pK_a, at any pH, a decrease of the pK_a by 1 unit raises the ratio of nitrite to nitrous acid by a factor of 10 (and an increase similarly decreases the ratio), and (2) the intracellular pH in environmental organisms can be substantially different than ambient conditions. For these reasons, nitrite's precise pK_a across temperatures in both freshwater and seawater salinities has a direct impact on revealing how nitrite speciates within organisms and in the environment at large.

The range of pK_a at 25 ºC from previous assessments exceeds 2 pH units (Table 4), which directly translates to a difference in the ratio of protonated to deprotonated nitrite by a factor of 100. Increasing the nitrous acid by a factor of 100 in turn commensurately increases its decomposition rate to NO and NO_2 by a factor of 10^4 given the second-order rate kinetics observed for this abiotic decomposition. This change in production rate will modify the intracellular concentration of NOx and thus its toxicity. Additionally, organisms operate at in-situ temperatures and salinities rather than idealized 25 ºC water with ionic

strength. The evaluation we provide here shows without the use of the appropriate pK_a, the actual speciation between nitrite and nitrous acid can be off by up to a factor of 4.

Furthermore, as the intracellular pH can differ from the ambient by multiple pH units (Siegumfeldt et al., 1999; Olsen et al., 2002), strictly speaking, the intracellular pH is the potentially more important parameter for defining the speciation nitric oxide toxicity for an individual cell. The temperature and salinity dependences of the pK_a reported here can be used for this evaluation. The pK_a also highlights the importance of preserving samples at alkaline pH to maintain nitrite as its conversion to gaseous products can lead to its ultimate loss in a bottle (or its abiotic oxidation to nitrate). Lastly, because protonated nitrous acid can likely diffuse across a cell membrane, the pK_a and resulting speciation may be important for quantifying the complete set of mechanisms by which fixed nitrogen is transported into and out of cells.

For example, even a seemingly small reduction in pH from 7.5 to 6.8 has been shown to radically change the microbially-mediated anaerobic cycling of nitrogen, leading to an accumulation of nitrite and elevated production of the greenhouse gas nitrous oxide (Baumann et al., 1997). Similarly, a reduction in pH from 7.5 to 6.5 can transform the interaction of microbial communities that cross-feed nitrite (Goldschmidt et al., 2018; Borer et al., 2020). Within these experiments, the driving mechanism of toxicity (directly the nitrous acid via proton decoupling versus the cytotoxicity of nitric oxide) remained elusive. Here we suggest that the mechanisms for nitrite toxicity likely derive from the abiotic protonation of nitrite at lower pH and the subsequent spontaneous decomposition of nitrous acid to nitric oxide that is the direct agent of toxicity (Zumft, 1993) or stress (Vardi et al., 2006; Schieler et al., 2019).

To our knowledge, this is the first attempt to strategically measure the pK_a of nitrous acid across environmentally relevant temperatures for freshwater, and the first measurements in seawater at any temperature. This is an important step to constrain the nitrite budget within aquatic systems, particularly as it is highly relevant for organism function. Further experiments are required to quantify the spontaneous decomposition of nitrous acid across environmental conditions to predict the potential accumulation of nitric oxide within cells and in the environment and to constrain the full nitrogen budget.

Acknowledgments

This study was funded by the Simons Foundation grant number #622065 and the National Science Foundation OCE-2142998 awarded to ARB. BB was supported by a fellowship of the Swiss National Science Foundation grant number P500PN_202842. EB was supported by the MIT UROP Office. RJW was supported by NSF Grants OCE-1923312 and OCE-2148468. The funders played no role in the study design, data collection, analysis, and interpretation of data, or the writing of this manuscript.

Competing interests

All authors declare no financial or non-financial competing interests.

Data and code availability

All extracted data and the underlying code for this study are available in Zenodo and can be accessed via this DOI: 10.5281/zenodo.10086128.

References

Abada, A., Beiralas, R., Narvaez, D., Sperfeld, M., Duchin-Rapp, Y., Lipsman, V., Yuda, L., Cohen, B., Carmieli, R., Ben-Dor, S., Rocha, J., Huang Zhang, I., Babbin, A.R., Segev, E., 2023. Aerobic bacteria produce nitric oxide via denitrification and promote algal population collapse. The ISME Journal 17, 1167–1183. doi:10.1038/s41396-023-01427-8

Babbin, A.R., Buchwald, C., Morel, F.M.M., Wankel, S.D., Ward, B.B., 2020. Nitrite oxidation exceeds reduction and fixed nitrogen loss in anoxic Pacific waters. Marine Chemistry 224, 103814. doi:10.1016/j.marchem.2020.103814

Babbin, A.R., Keil, R.G., Devol, A.H., Ward, B.B., 2014. Organic matter stoichiometry, flux, and oxygen control nitrogen loss in the ocean. Science 344, 406–408. doi:10.1126/science.1248364

Babbin, A.R., Peters, B.D., Mordy, C.W., Widner, B., Casciotti, K.L., Ward, B.B., 2017. Multiple metabolisms constrain the anaerobic nitrite budget in the Eastern Tropical South Pacific. Global Biogeochemical Cycles 31, 258–271. doi:10.1002/2016GB005407

Babbin, A.R., Tamasi, T., Dumit, D., Weber, L., Rodríguez, M.V.I., Schwartz, S.L., Armenteros, M., Wankel, S.D., Apprill, A., 2021. Discovery and quantification of anaerobic nitrogen metabolisms among oxygenated tropical Cuban stony corals. The ISME Journal 15, 1222–1235. doi:10.1038/s41396-020-00845-2

Bates, R.G., Calais, J.G., 1981. Thermodynamics of the dissociation of Bis H+ in seawater from 5 to 40°C. Journal of Solution Chemistry 10, 269–279. doi:10.1007/BF00645016

Baumann, B., Van Der Meer, J.R., Snozzi, M., Zehnder, A.J.B., 1997. Inhibition of denitrification activity but not of mRNA induction in Paracoccus dentrificans by nitrite at a suboptimal pH. Antonie van Leeuwenhoek, International Journal of General and Molecular Microbiology 72, 183–189. doi:10.1023/A:1000342125891

Borer, B., Ciccarese, D., Johnson, D., Or, D., 2020. Spatial organization in microbial range expansion emerges from trophic dependencies and successful lineages. Communications Biology 3, 1–10. doi:10.1038/s42003-020-01409-y

Ciccarese, D., Micali, G., Borer, B., Ruan, C., Or, D., Johnson, D.R., 2022. Rare and localized events stabilize microbial community composition and patterns of spatial self-organization in a fluctuating environment. The ISME Journal 1–11. doi:10.1038/s41396-022-01189-9

Ciccarese, D., Tantawi, O., Zhang, I.H., Plata, D., Babbin, A.R., 2023. Microscale dynamics promote segregated denitrification in diatom aggregates sinking slowly in bulk oxygenated seawater. Communications Earth & Environment 4, 1–13. doi:10.1038/s43247-023-00935-x

Clegg, S.L., Whitfield, M., 1995. A chemical model of seawater including dissolved ammonia and the stoichiometric dissociation constant of ammonia in estuarine water and seawater from −2 to 40°C. Geochimica et Cosmochimica Acta 59, 2403–2421. doi:10.1016/0016-7037(95)00135-2

Crutzen, P.J., 1979. The Role of NO and NO2 in the Chemistry of the Troposphere and Stratosphere. Annual Review of Earth and Planetary Sciences 7, 443–472. doi:10.1146/annurev.ea.07.050179.002303

da Silva, G., Kennedy, E.M., Dlugogorski, B.Z., 2006. Ab Initio Procedure for Aqueous-Phase pKa Calculation: The Acidity of Nitrous Acid. The Journal of Physical Chemistry A 110, 11371–11376. doi:10.1021/jp0639243

das Graças Gomes, M., da S.S. Borges, S., Lopes, L.G.F., Franco, D.W., 1993. UV-visible spectrum of nitrous acid in solution: pKa determination and analytical applications. Analytica Chimica Acta 282, 81–85. doi:10.1016/0003-2670(93)80354-N

DelValls, T.A., Dickson, A.G., 1998. The pH of buffers based on 2-amino-2-hydroxymethyl-1,3-propanediol ('tris') in synthetic sea water. Deep Sea Research Part I: Oceanographic Research Papers 45, 1541–1554. doi:10.1016/S0967-0637(98)00019-3

Dickson, A.G., Camões, M.F., Spitzer, P., Fisicaro, P., Stoica, D., Pawlowicz, R., Feistel, R., 2015. Metrological challenges for measurements of key climatological observables. Part 3: seawater pH. Metrologia 53, R26. doi:10.1088/0026-1394/53/1/R26

Goldschmidt, F., Regoes, R.R., Johnson, D.R., 2018. Metabolite toxicity slows local diversity loss during expansion of a microbial cross-feeding community. ISME Journal 12, 136–144. doi:10.1038/ismej.2017.147

Gruber, N., Galloway, J.N., 2008. An Earth-system perspective of the global nitrogen cycle. Nature 451, 293–296. doi:10.1038/nature06592

Ives, D.J.G., Moseley, P.G.N., 1976. Derivation of thermodynamic functions of ionisation from acidic dissociation constants. The sigma plot method vis-à-vis polynomial regression procedures. Journal of the Chemical Society, Faraday Transactions 1: Physical Chemistry in Condensed Phases 72, 1132–1143. doi:10.1039/F19767201132

Khoo, K.H., Culberson, C.H., Bates, R.G., 1977. Thermodynamics of the dissociation of ammonium ion in seawater from 5 to 40°C. Journal of Solution Chemistry 6, 281–290. doi:10.1007/BF00645459

Klemenc, A., Hayek, E., 1929. Zur Kenntnis der Dissoziationskonstante der salpetrigen Säure. Monatshefte für Chemie und verwandte Teile anderer Wissenschaften 53, 407–412. doi:10.1007/BF01521803

Lee, P.A., Mikucki, J.A., Foreman, C.M., Priscu, J.C., DiTullio, G.R., Riseman, S.F., Mora, S.J., Wolf, C.F., Kester, L., 2004. Thermodynamic Constraints on Microbially Mediated Processes in Lakes of the McMurdo Dry Valleys, Antarctica. Geomicrobiology Journal 21, 221–237. doi:10.1080/01490450490275884

Lilja, E.E., Johnson, D.R., 2016. Segregating metabolic processes into different microbial cells accelerates the consumption of inhibitory substrates. ISME Journal 10, 1568–1578. doi:10.1038/ismej.2015.243

Lomas, M.W., Lipschultz, F., 2006. Forming the primary nitrite maximum: Nitrifiers or phytoplankton? Limnology and Oceanography 51, 2453–2467. doi:10.4319/lo.2006.51.5.2453

Lumme, P., Tummavuori, J., 1965. Nitrous Acid in Aqueous Sodium Perchlorate Solutions at 25 C. Acta Chemica Scandinavica 19, 617–621.

Millero, F.J., 2013. Chemical Oceanography, 4th ed. CRC Press, Boca Raton. doi:10.1201/b14753

Millero, F.J., 1995. Thermodynamics of the carbon dioxide system in the oceans. Geochimica et Cosmochimica Acta 59, 661–677. doi:10.1016/0016-7037(94)00354-O

Millero, F.J., Plese, T., Fernandez, M., 1988. The dissociation of hydrogen sulfide in seawater1. Limnology and Oceanography 33, 269–274. doi:10.4319/lo.1988.33.2.0269

Olsen, K.N., Budde, B.B., Siegumfeldt, H., Rechinger, K.B., Jakobsen, M., Ingmer, H., 2002. Noninvasive Measurement of Bacterial Intracellular pH on a Single-Cell Level with Green Fluorescent Protein and Fluorescence Ratio Imaging Microscopy. Applied and Environmental Microbiology 68, 4145–4147. doi:10.1128/AEM.68.8.4145-4147.2002

Park, J.Y., Lee, Y.N., 1988. Solubility and decomposition kinetics of nitrous acid in aqueous solution. The Journal of Physical Chemistry 92, 6294–6302. doi:10.1021/j100333a025

Paulsen, M.-L., Dickson, A.G., 2020. Preparation of 2-amino-2-hydroxymethyl-1,3-propanediol (TRIS) pHT buffers in synthetic seawater. Limnology and Oceanography: Methods 18, 504–515. doi:10.1002/lom3.10383

Powers, S.M., Labou, S.G., Baulch, H.M., Hunt, R.J., Lottig, N.R., Hampton, S.E., Stanley, E.H., 2017. Ice duration drives winter nitrate accumulation in north temperate lakes. Limnology and Oceanography Letters 2, 177–186. doi:10.1002/lol2.10048

Riordan, E., Minogue, N., Healy, D., O'Driscol, P., Sodeau, J.R., 2005. Spectroscopic and Optimization Modeling Study of Nitrous Acid in Aqueous Solution. The Journal of Physical Chemistry A 109, 779–786. doi:10.1021/jp040269v

Schieler, B.M., Soni, M.V., Brown, C.M., Coolen, M.J.L., Fredricks, H., Van Mooy, B.A.S., Hirsh, D.J., Bidle, K.D., 2019. Nitric oxide production and antioxidant function during viral infection of the coccolithophore Emiliania huxleyi. The ISME Journal 13, 1019–1031. doi:10.1038/s41396-018-0325-4

Schmid, H., Marchgraber, R., Dunkl, F., 1937. Messungen der elektrolytischen Leitfähigkeit im Dienste der Thermodynamik der Zwischenreaktionen. Zeitschrift Für Elektrochemie Und Angewandte Physikalische Chemie 43, 337–340. doi:10.1002/bbpc.19370430518

Schümann, M., 1900. Zur Kenntniss des Diazotirungsprocesses und der salpetrigen Säure. Berichte Der Deutschen Chemischen Gesellschaft 33, 527–533. doi:10.1002/cber.19000330183

Siegumfeldt, H., Rechinger, K.B., Jakobsen, M., 1999. Use of fluorescence ratio imaging for intracellular pH determination of individual bacterial cells in mixed cultures. Microbiology 145, 1703–1709. doi:10.1099/13500872-145-7-1703

Snoeyink, V., Jenkins, D., 1991. Water Chemistry. Wiley.

Stephens, E.R., Hanst, P.L., Doerr, R.C., Scott, W.E., 1956. Reactions of Nitrogen Dioxide and Organic Compounds in Air. Industrial & Engineering Chemistry 48, 1498–1504. doi:10.1021/ie51400a036

Ulloa, O., Canfield, D.E., DeLong, E.F., Letelier, R.M., Stewart, F.J., 2012. Microbial oceanography of anoxic oxygen minimum zones. Proceedings of the National Academy of Sciences 109, 15996–16003. doi:10.1073/pnas.1205009109

Vardi, A., Formiggini, F., Casotti, R., Martino, A.D., Ribalet, F., Miralto, A., Bowler, C., 2006. A Stress Surveillance System Based on Calcium and Nitric Oxide in Marine Diatoms. PLOS Biology 4, e60. doi:10.1371/journal.pbio.0040060

Vassian, E.G., Eberhardt, W.H., 1958. The Spectrophotometric Determination of the Dissociation Constant of a Cadmium–Nitrite Complex.. The Journal of Physical Chemistry 62, 84–87. doi:10.1021/j150559a022

Vincent, W.F., Downes, M.T., Vincent, C.L., 1981. Nitrous oxide cycling in Lake Vanda, Antarctica. Nature 292, 618–620. doi:10.1038/292618a0

Wilbert, S.A., Newman, D.K., 2022. The contrasting roles of nitric oxide drive microbial community organization as a function of oxygen presence. Current Biology 32, 5221-5234.e4. doi:10.1016/j.cub.2022.10.008

Zakem, E.J., Al-Haj, A., Church, M.J., van Dijken, G.L., Dutkiewicz, S., Foster, S.Q., Fulweiler, R.W., Mills, M.M., Follows, M.J., 2018. Ecological control of nitrite in the upper ocean. Nature Communications 9, 1206. doi:10.1038/s41467-018-03553-w

Zhao, R., Babbin, A.R., Roerdink, D.L., Thorseth, I.H., Jørgensen, S.L., 2023. Nitrite accumulation and anammox bacterial niche partitioning in Arctic Mid-Ocean Ridge sediments. ISME Communications 3, 1–14. doi:10.1038/s43705-023-00230-y

Zumft, W.G., 1993. The biological role of nitric oxide in bacteria. Archives of Microbiology 160, 253–264. doi:10.1007/BF00292074

Tables

*Table 1**: Composition of the synthetic seawater.** This formulation does not contain any carbonates or boric acid to restrict interference of their buffering capacity with our measurements. Recipe adapted from Frank J. Millero: "Chemical Oceanography" (Millero, 2013).*

Component	**Supplier**	**CAS#**	**Mass**
NaCl	Sigma–Aldrich	7647-14-5	248.33 g
Na_2SO_4	Sigma–Aldrich	7757-82-6	41.49 g
KCl	Sigma–Aldrich	7447-40-7	7.22 g
KBr	Acros Organics	7758-02-3	1.04 g
NaF	VWR Chemicals BDH	7681-49-4	30 mg
$MgCl_2 \times 6\ H_2O$	Sigma–Aldrich	7791-18-6	111.09 g
$CaCl_2 \times 2\ H_2O$	Sigma–Aldrich	10035-04-8	11.87 g
$SrCl_2 \times 6\ H_2O$	Acros Organics	10025-70-4	250 mg

Table 2: Regression intercepts and slopes for all calibrations and temperatures following the linear equation $EMF_{(t)} = q_{(t)} + m_{(t)} \times pH_{(t)}$ (Eq. 5). The individually measured intercepts are reported for both freshwater and artificial seawater with the subscript I. In addition, the intercepts calculated from a regression across temperatures (Eq. 6) are reported with subscript R. Calibration slopes (m) are reported for the individual measurements (I) and regressions (R) when using Eq. 7. For comparison, the slope of an optimal electrode (m_{Nernst}) is also reported. At 10 °C, values for the individual intercept and slope are missing due to the unreliable behavior of the electrode during calibration. All intercepts are in units of mV, all slopes are in units of mV pH^{-1}. FW indicates freshwater and ASW denotes artificial seawater.

T (°C)	5	10	15	20	25	30	35
$q_{FW,I}$	379.31	---	394.12	403.06	408.98	418.25	426.49
$q_{FW,R}$	378.92	386.75	394.58	402.42	410.26	418.09	425.93
$q_{ASW,I}$	384.64	388.31	395.31	400.35	403.68	410.53	415.32
$q_{ASW,R}$	384.21	389.39	394.56	399.73	404.91	410.08	415.25
$m_{FW,I}$	-53.53	---	-55.91	-57.27	-58.21	-59.52	-60.55
$m_{FW,R}$	-53.58	-54.76	-55.93	-57.11	-58.28	-59.46	-60.63
m_{Nernst}	-55.19	-56.18	-57.18	-58.17	-59.16	-60.15	-61.14

Table 3: Extracted EMF at the half equivalence point and converted to a pK_a on the NBS scale for freshwater experiments and on the total scale (T) for seawater experiments.

Temperature		5°C	10°C	15°C	20°C	25°C	30°C	35°C
Freshwater	N	4	3	4	2	3	3	2
	T_{meas}	5.30±0.12	10.14±0.01	15.03±0.02	20.05±0.01	25.09±0.03	30.06±0.03	34.99±0.04
	EMF	204.41±0.18	211.76±0.12	217.15±0.06	222.35±0.12	227.5±0.08	231.62±0.19	235.47±0.48
	$pK_{a,NBS}$	3.257±0.003	3.196±0.002	3.172±0.001	3.153±0.002	3.136±0.001	3.136±0.003	3.141±0.008
Seawater	N	4	4	4	4	4	4	2
	T_{meas}	5.22±0.02	10.09±0.02	14.89±0.12	20.04±0.03	25.16±0.07	30.12±0.03	35.00±0.03
	EMF	217.49±0.08	224.2±0.20	230.44±0.27	236.11±0.21	241.19±0.51	245.24±0.39	248.23±0.35
	$pK_{a,T}$	3.119±0.001	2.997±0.004	2.948±0.005	2.876±0.004	2.788±0.009	2.780±0.007	2.756±0.006

511 *Table 4: Previously determined nitrous acid dissociation constants.* NR, not reported.

pK_a	T (ºC)	Method	Reference
3.14 ± 0.001	25	Potentiometry	Our data
3.16 ± 0.51	25	---	Mean previously reported 25 ºC values
3.16	25	Spectroscopy	(da Silva et al., 2006)
3.24 ± 0.03	22.0	Calculated from decomposition kinetics	(Park and Lee, 1988)
3.34	25	Conductivity	(Schümann, 1900)
3.29	25	Conductivity	(Schmid et al., 1937)
3.28	25	Spectroscopy	(Vassian and Eberhardt, 1958)
3.15	25	Potentiometry	(Lumme and Tummavuori, 1965)
2.8 ± 0.1	NR	Spectroscopy	(Riordan et al., 2005)
3.34 ± 0.02	12.5	Conductivity	(Klemenc and Hayek, 1929)
3.22 ± 0.02	30	Conductivity	(Klemenc and Hayek, 1929)
2.3 ± 0.2	25	Spectroscopy + Potentiometry	(das Graças Gomes et al., 1993)
4.5	25	NR	(Snoeyink and Jenkins, 1991)

512

513

Table 5: Fitted parameters relating measured pK_a to the temperature and derived thermodynamic parameters. We converted temperatures to Kelvin prior to fitting Eq. 11 of the form $pK_a = \frac{A}{T} + B\ ln(T) + C$ to the pK_a values. Fitted coefficients are converted to thermodynamic parameters using the coefficients in Eq. 10 and listed as "least squares". FW and ASW stand for freshwater and artificial seawater, respectively.

Fitted Value	**A**	**B**	**C**
FW Fit	11328	37.613	-249.16
ASW Fit	15168	48.245	-322.94
Derived parameter	ΔH_0^o**(kcal mol^{-1})**	ΔC_P **(kcal K^{-1} mol^{-1})**	ΔS_0^o **(kcal K^{-1} mol^{-1})**
FW Least-Squares	51.83	-0.17	1.14
FW Sigma plot	52.53	-0.18	0.99
ASW Least-Squares	69.41	-0.22	1.48
ASW Sigma plot	75.32	-0.24	1.38

Figures

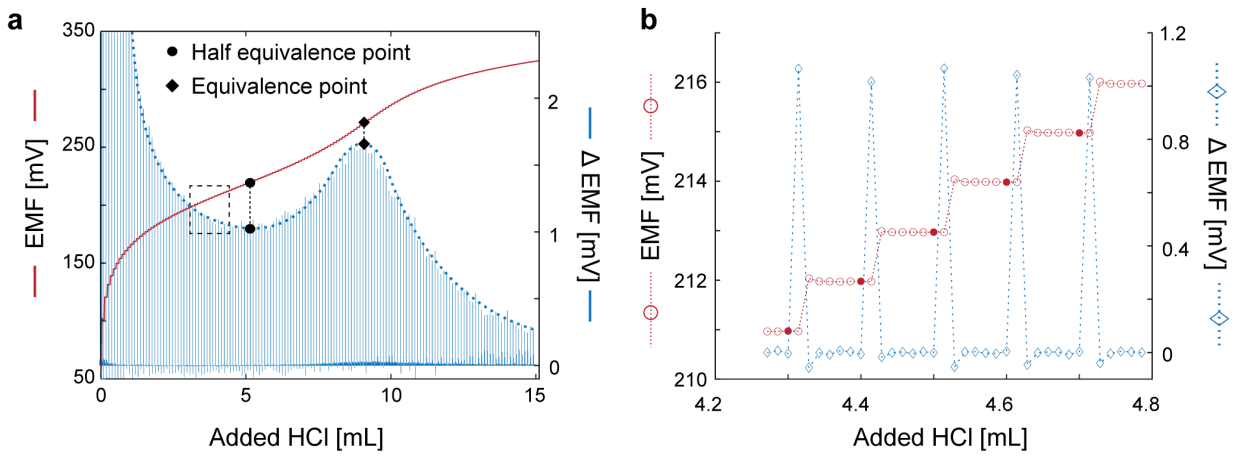

Fig. 1: Example measured EMF (red) and the difference between subsequent EMF measurements (blue) as a function of the added titrant (HCl). *a) The two inflection points of the titration curve (where the change in measured EMF is minimal and maximal, respectively) correspond to the half equivalence point (where the pH equals the pK_a) and equivalence point of the titration (where the total added titrant equals the amount of titrate). We extract the titration half equivalence point using a combination of numerical and analytical approaches (see Methods section) to improve the precision. b) Detailed view of the data for the section outlined by the dashed rectangle in panel a. After injection of titrant, the EMF rapidly stabilized to within the calibrated accuracy of the electrode (±0.01 mV). For the final analysis, only the last measurement prior to the injection of the new titrant was used for the extraction of the EMF at the half equivalence point (filled red data point in the inset).*

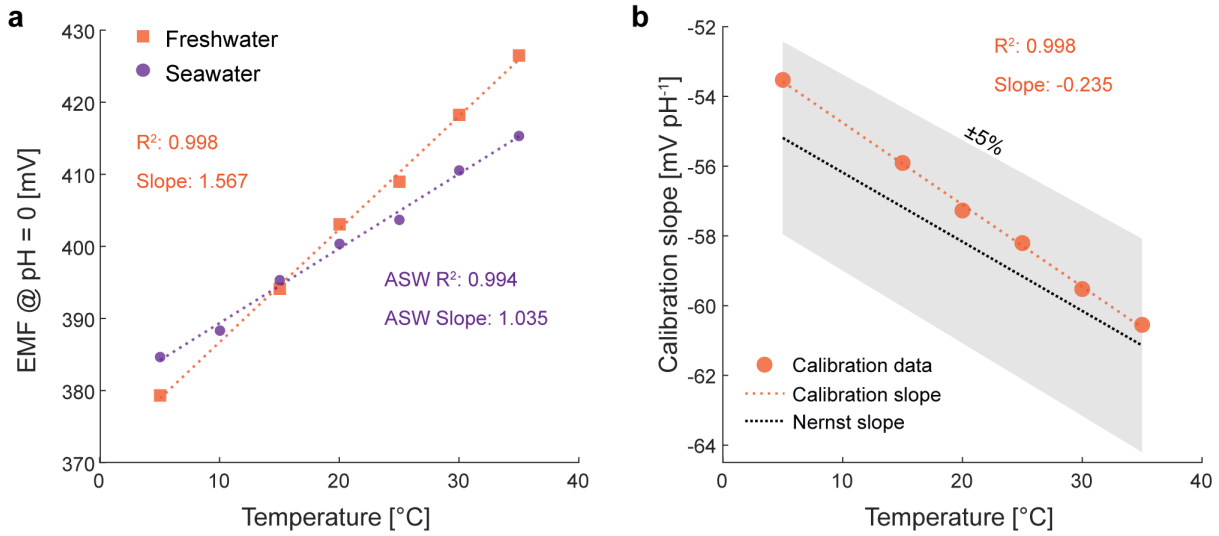

Fig. 2: Visualization of the calibration for both freshwater and saltwater*. a) Calculated intercept of the freshwater calibration which represents the EMF at pH 0. Measured EMF of the one-point calibration corrected to pH 0 (using the freshwater slope shown in panel b) for the saltwater calibration. b) Predicted calibration slopes for all temperatures and the temperature dependence of the calibration slopes. The dashed line shows the temperature dependence of a Nernstian electrode including a deviation of ±5% indicated by the shaded area (the accepted envelope of an electrode).*

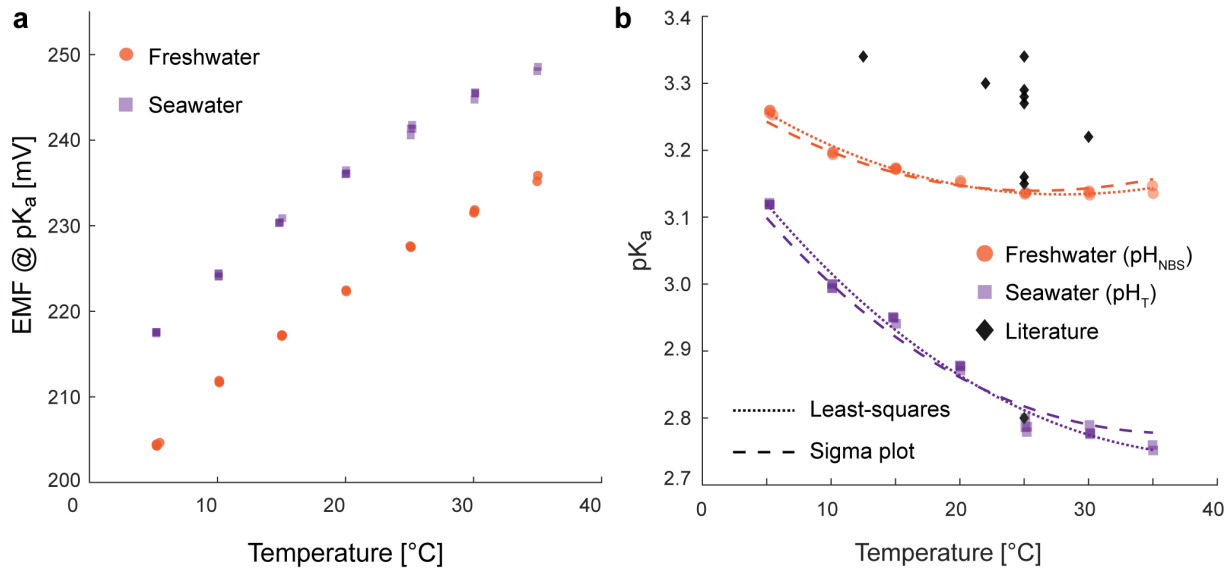

Fig. 3: Extracted EMF at the half equivalence point and converted to pK_a. *a) Extracted EMF at the half equivalence point for both the freshwater and seawater experiments across temperatures. b) Measured EMF at the half equivalence point converted to pH on the NBS scale for freshwater titrations and on the total scale for seawater titrations. Black diamonds indicate literature values presented in Table 4.*

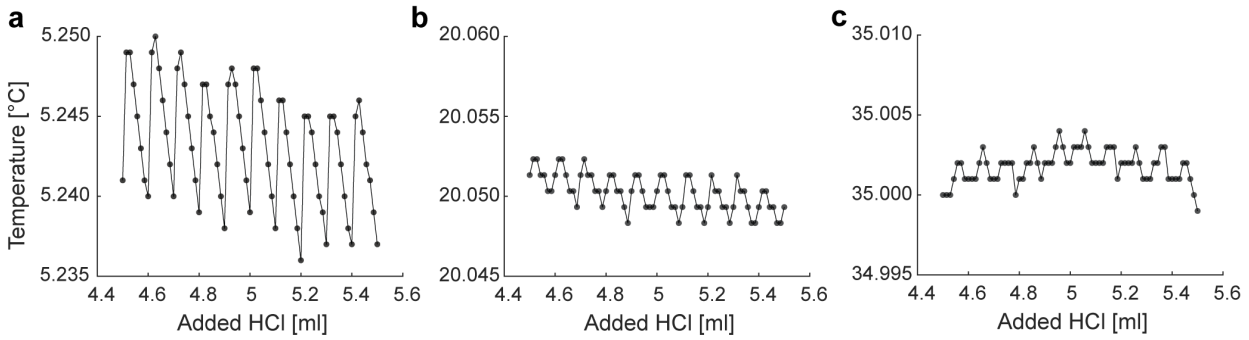

Fig. 4: Recorded temperature inside the titration beaker. *a) At 5 °C, the room-temperature titrant combined with the heat released due to exothermic dilution elevates the temperature slightly above the targeted 5 °C. b) At 20 °C, the room-temperature titrant does not significantly influence the temperature at each injection but the exothermic dilution effect elevates the temperature ~0.05 °C above the targeted value of 20 °C. c) At 35 °C, the heat of dilution cancels out the potential cooling effect of the room temperature titrant. The residual spread of the measured data is close to the accuracy of the temperature probe (±0.001 °C)*